

6B.3 PROBING THE SPATIOTEMPORAL STRUCTURE OF HYDROMETEORS IN INDIAN MONSOON DEPRESSIONS

Kieran M. R. Hunt*

Andrew G. Turner

February 1, 2016

1 INTRODUCTION

Indian monsoon depressions (IMDs) are synoptic scale disturbances that originate near the head of the Bay of Bengal or in the Indian monsoon trough region. With a typical frequency of 2-5 per summer, and an average duration of 4-6 days, they are an important feature of the Indian monsoon, capable of providing very heavy precipitation across much of northern India (Godbole, 1977; Stano *et al.*, 2002; Hunt *et al.*, 2016). It is therefore crucial to have a clear understanding of the hydrometeor structure and moist thermodynamic processes of these events. Short and Nakamura (2000) and Fu and Liu (2001) provided the first analyses of the vertical structure of rainfall rates in the tropics using satellite data, preceding the case study of the three 1999 depressions by Stano *et al.* (2002). Since then, there have been numerous further studies using the Tropical Rainfall Measuring Mission (TRMM), but none exploiting the depth of such satellite data on the nearly forty IMDs that have occurred since the launch of TRMM. Recently, Bowman and Fowler (2015) used TRMM to examine the diurnal structure of tropical cyclones showing that precipitation within 500 km of the centre had a diurnal cycle with a maximum in the early morning.

We remain, therefore, without a verified understanding of the moist processes that occur in IMDs. Whilst it has been known for some time that the maximum surface precipitation is to be found several hundred kilometres southwest of the depression centre (e.g. Ramanathan and Ramakrishnan, 1933), there is no certainty on the generating mechanism and several prevailing theories result: the westward axial tilt of the core with height, collocation with a lower-troposphere convergence maximum, cyclonic mixing of warm monsoon circulation with cool southwesterlies from the Bay of Bengal, or even some combination of these. More recently, Yoon and Chen (2005) suggested that this asymmetry was a consequence of IMD water vapour flux convergence coupling with longer period modes of monsoon variability, but showed only that these intraseasonal modes could enhance or suppress the IMD rainfall, not affect its location.

2 COMPOSITE STRUCTURE

Using the tracking algorithm and data outlined in Hunt *et al.* (2016), we outlined 34 depressions concurrent with the Tropical Rainfall Measuring Mission (TRMM Kummerow *et al.*, 1998), and 12 with the CloudSat mission (Stephens *et al.*, 2002); these are identified in Fig. 1 as white and red (where they overlap) respectively. These data were then used in conjunction with the suite of products available from both Cloud-

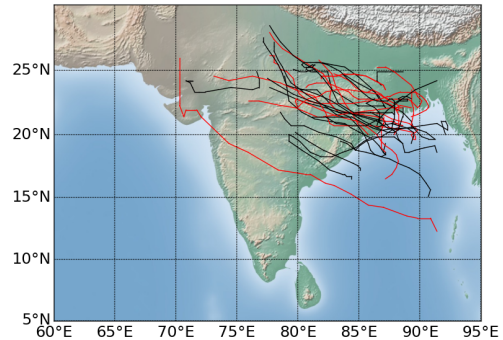


Figure 1: The paths of the 12 IMDs that fell within both the CloudSat and TRMM periods (red), and the 22 further depressions that were within just the TRMM period (black).

Sat and TRMM to generate composite structures of a number of fields for IMDs.

The resulting three-dimensional composite may have an insufficient sample size for analysis (this is particularly the case with the nadir-only CloudSat retrievals). To overcome this, we boost sample size by collapsing the azimuthal dimension and treating the composite data as a function only of radius and height. This introduces a degeneracy that we can exploit to examine an asymmetry of our choice. The dominant mode of spatial asymmetry in IMDs is caused by the presence of the Himalayas (Hunt *et al.*, 2016; Hunt and Parker, 2015), and so we define the pseudoradial coordinate, with magnitude equal to the radius and sharing the sign of the normalised latitude (i.e., negative south of the centre, and positive to the north).

An example result from this process is composite cloud type (Fig. 2), which shows deep convection present to the south of the centre (collocated with the surface precipitation maximum) contrasting dense orographic stratus in the north. Further away from the centre, in the south, the cloud structure simply resembles that expected of a typical tropical atmosphere.

Other important results from the composite are: that the modal raindrop size is mostly uniform throughout the lower and mid-troposphere indicating the IMD is well mixed with height in these areas, in contrast it increases with height at the centre, indicating strong forced ascent; high graupel and snow densities located across the IMD, with maxima above the surface precipitation maximum further establishing the presence of deep convection there; a latent heating maximum of 2 K hr^{-1} located at an altitude of 3 km, also above the precipitation maximum, and below the radiative heating maximum of 0.2 K hr^{-1} at an altitude of 15 km.

*Department of Meteorology, University of Reading, Reading, UK; email: k.hunt@pgr.reading.ac.uk

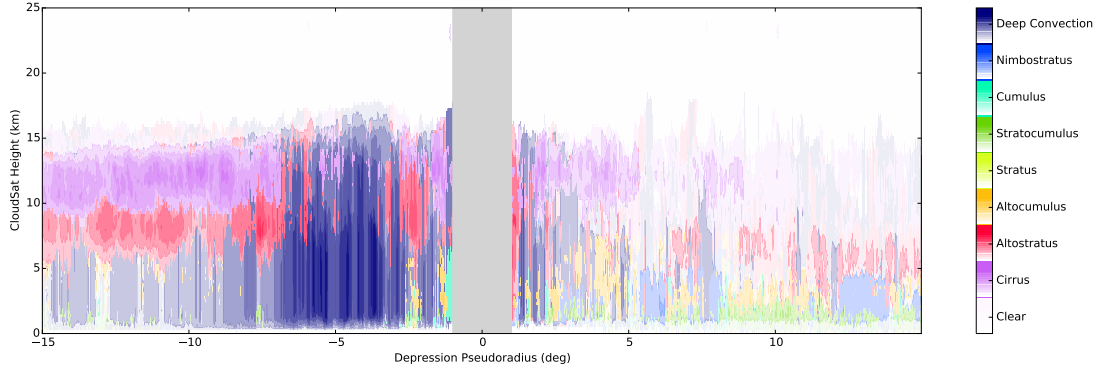


Figure 2: Modal cloud scenario in the composite, determined by CloudSat 2B-CLDCLASS. Differing hues represent varying cloud types, with the transparency in each case proportional to the ratio of the modal value and the number of overpasses up to a value of 0.5. Parts of the composite not comprising at least ten satellite overpasses are not shown. We remind the reader that CloudSat height is referenced above the Earth's surface rather than necessarily the geoid.

3 CASE STUDY

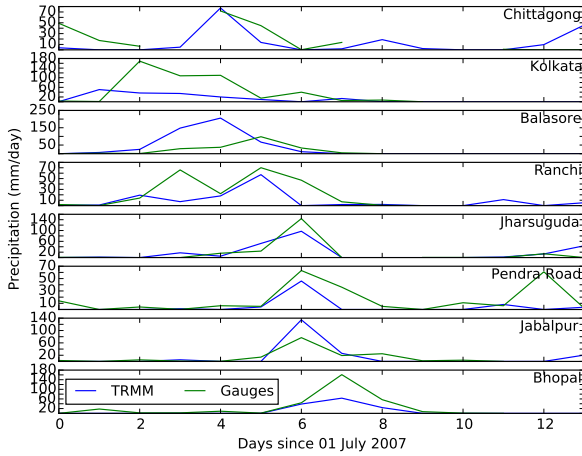


Figure 3: Daily precipitation (mm day^{-1}) for eight selected stations along the path of the depression in early July 2007, approximately from east to west. Gauge values are given in green, TRMM 3B42 estimates are given in blue.

The nature of this research prompts a validation of the satellite products, both with each other and with independent data. For this purpose, we select a case study where TRMM and CloudSat overpasses intersect near an IMD centre within a short timeframe. The best such example was the IMD of early July 2007: the overpass intersection was separated by 62 minutes at a distance of just 96 km from the depression centre. This provided us with a snapshot of a typical IMD with which to compare the composite, as well as allowing us to validate the TRMM 3B42 product against station-based gauge data (a selection of these data are shown in Fig. 3). The salient results of this section were that TRMM underestimates the high intensity rainfall associated with IMDs by as much as 50%, and that individual IMDs look reasonably similar to the composite, perhaps surprising given the highly variable nature of hydrometeor-related fields.

4 DIURNAL VARIABILITY

Exploration of composite TRMM 3B42 IMD surface rainfall data (split by time of day into three-hourly blocks) indicates that the near-central precipitation maximum varies diurnally with a maximum near local dawn. In contrast, whilst the weaker precipitation in the flanks also seems to vary diurnally but with a maximum at local dusk. This was quantified by fitting to the data a sum of two arbitrarily-phased two-dimensional Gaussian functions with some climatological offset (or residual), of the form:

$$P(x, y) = P_{\text{residual}}(x, y) + \sum_{n=0}^1 A_n \exp(-[x - x_{o,n} \quad y - y_{o,n}] \begin{pmatrix} \cos^2 \theta_n + \frac{\sin^2 \theta_n}{2\sigma_{x,n}^2} & \frac{\sin 2\theta_n}{4\sigma_{x,n}^2} - \frac{\sin 2\theta_n}{4\sigma_{y,n}^2} \\ \frac{\sin 2\theta_n}{4\sigma_{x,n}^2} - \frac{\sin 2\theta_n}{4\sigma_{y,n}^2} & \frac{\sin^2 \theta_n}{2\sigma_{x,n}^2} + \frac{\cos^2 \theta_n}{2\sigma_{y,n}^2} \end{pmatrix} \begin{bmatrix} x - x_{o,n} \\ y - y_{o,n} \end{bmatrix}), \quad (1)$$

where P is the observed spatial distribution of the precipitation, P_{residual} is the difference between the observed rainfall and the fitted function, n is an index for the two Gaussian functions, σ_x and σ_y refer to the standard deviation of the Gaussian along the x and y axes respectively, (x_o, y_o) are the coordinates of the centre of the Gaussian, and θ is its rotational phase. The resulting amplitudes of each Gaussian as a function of time of day is given in Fig. 4. We recover two modes that are roughly in antiphase, and EOF analysis confirms that this diurnal contrast is the dominant mode of precipitation variability in IMDs. Further work is required to determine whether these two modes are coupled, and if so, how.

Overall, our analysis suggests that the reason for the surface rainfall asymmetry is the cyclonic mixing of cool air from the Arabian Sea and warmer, moist monsoon air from the peninsula, causing uplift of the latter.

References

- Bowman KP, Fowler MD. 2015. The diurnal cycle of precipitation in tropical cyclones. *J. Climate* **28**: 5325–5334, doi: 10.1175/JCLI-D-14-00804.1.
- Fu Y, Liu G. 2001. The variability of tropical precipitation profiles and its impact on microwave brightness temperatures as inferred from TRMM data. *J. Appl. Meteor.*

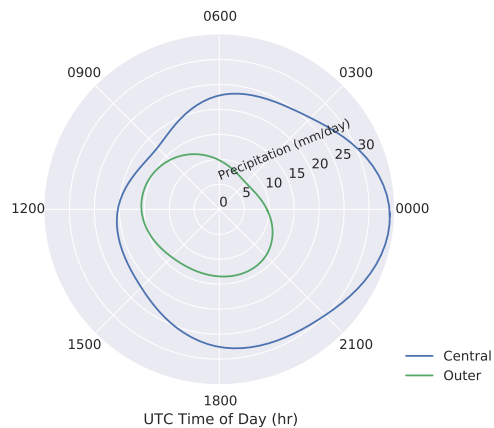


Figure 4: Amplitudes of the two diurnal modes of surface precipitation (mm day^{-1}) in the rotated composite, derived from TRMM 3B42.

40: 2130–2143, doi:10.1175/1520-0450(2001)040<2130:TVOTPP>2.0.CO;2.

Godbole R. 1977. The composite structure of the monsoon depression. *Tellus* **29**: 25–40.

Hunt KMR, Parker DJ. 2015. The movement of Indian monsoon depressions by interaction with image vortices near the Himalayan wall. *Quart. J. Roy. Meteor. Soc.* Submitted.

Hunt KMR, Turner AG, Inness PM, Parker DE, Levine RC. 2016. On the structure and dynamics of Indian monsoon depressions. *Mon. Wea. Rev.* Accepted.

Hurley JV, Boos WR. 2015. A global climatology of monsoon low pressure system. *Quart. J. Roy. Meteor. Soc.* **141**: 1049–1064, doi:10.1002/qj.2447.

Krishnamurthy V, Shukla J. 2007. Intraseasonal and seasonally persisting patterns of Indian monsoon rainfall. *J. Climate* **20**: 3–20, doi:10.1175/JCLI3981.1, URL <http://dx.doi.org/10.1175/JCLI3981.1>.

Kummerow C, Barnes W, Kozu T, Shiue J, Simpson J. 1998. The tropical rainfall measuring mission (TRMM) sensor package. *J. Atmos. Oceanic Technol.* **15**: 809–817, doi:10.1175/1520-0426(1998)015<0809:TTRMMT>2.0.CO;2.

Ramanathan KR, Ramakrishnan KP. 1933. The Indian southwest monsoon and the structure of depressions associated with it. *Mem. Ind. Meteor. Dept.* **26**: 13–36.

Saha K, Sanders F, Shukla J. 1981. Westward propagating predecessors of monsoon depressions. *Mon. Wea. Rev.* **109**: 330–343.

Sarker RP, Choudhary A. 1988. A diagnostic study of monsoon depressions. *Mausam* **39**: 9–18.

Short DA, Nakamura K. 2000. TRMM radar observations of shallow precipitation over the tropical oceans. *J. Climate* **13**: 4107–4124, doi:10.1175/1520-0442(2000)013<4107:TROOSP>2.0.CO;2.

Sikka DR. 1977. Some aspects of the life history, structure and movement of monsoon depressions. *Pure Appl. Geophys.* **115**: 1501–1529.

Stano G, Krishnamurti TN, Vijaya Kumar TSV, Chakraborty A. 2002. Hydrometeor structure of a composite monsoon depression using the TRMM radar. *Tellus A* **54**: 370–381, doi:10.1034/j.1600-0870.2002.01330.x.

Stephens GL, Vane DG, Boain RJ, Mace GG, Sassen K, Wang Z, Illingworth AJ, O'Connor EJ, Rossow WB, Durden SL, et al. 2002. The CloudSat mission and the A-Train: a new dimension of space-based observations of clouds and precipitation. *Bull. Amer. Meteor. Soc.* **83**(12): 1771–1790.

Yoon JH, Chen TC. 2005. Water vapor budget of the Indian monsoon depression. *Tellus A* **57**(5): 770–782, doi:10.1111/j.1600-0870.2005.00145.x, URL <http://dx.doi.org/10.1111/j.1600-0870.2005.00145.x>.